J. Fluid Mech. (2009), *vol.* 633, *pp.* 285–309.
doi:10.1017/S0022112009007034 Printed in the United Kingdom

The early stages of shallow flows in an inclined flume

MATTEO ANTUONO[1], ANDREW J. HOGG[2]† AND MAURIZIO BROCCHINI[3]

[1]DICAT, Università degli Studi di Genova, via Montallegro 1, 16145 Genova, Italy

[2]Centre for Environmental & Geophysics Flows, School of Mathematics, University of Bristol, University Walk, Bristol BS8 1TW, UK

[3]Istituto di Idraulica e Infrastrutture Viarie, Università Politecnica delle Marche, via Brecce Bianche 12, 60131 Ancona, Italy

(Received 27 February 2008 and in revised form 11 March 2009)

The motion of an initially quiescent shallow layer of fluid within an impulsively tilted flume is modelled using the nonlinear shallow water equations. Analytical solutions for the two-dimensional flow are constructed using the method of characteristics and, in regions where neither of the characteristic variables is constant, by adopting hodograph variables and using the Riemann construction for the solution. These solutions reveal that the motion is strongly influenced by the impermeable endwalls of the flume. They show that discontinuous solutions emerge after some period following the initiation of the flow and that for sufficiently long flumes there is a moving interface between wetted and dry regions. Using the hodograph variables we are able to track the evolution of the flow analytically. After the discontinuities develop, we also calculate the velocity and height fields by using jump conditions to express conservation of mass and momentum across the shock and thus we show how the hydraulic jump moves within the domain and how its magnitude grows. In addition to providing the behaviour of the flow in this physical scenario, this unsteady solution also provides an important test case for numerical algorithms designed to integrate the shallow water equations.

1. Introduction

Liquid sloshing is a significant problem in the transportation of fuels and for many marine applications. The induced fluid motion can affect the dynamics and stability of the transporting vessel and the fluid impacts place significant loads on the containing structure (see, for example, Faltinsen, Landrini & Greco 2004). Additionally in heavy seas, a ship may receive relatively large volumes of seawater on its deck. This 'green' water may then slosh around the deck at relatively high velocities, potentially causing damage to equipment and structures (Lee, Zhou & Cao 2002). The surface deformation of the fluid layer is particularly violent when the layer is relatively shallow. In this scenario the amplitude of the wave motion may become comparable with the fluid depth and hence the dynamics are strongly nonlinear (Huang & Hsiung 1996). Furthermore steep and broken waves form, leading to hydraulic jumps, which translate throughout the domain. Such motions were documented in experiments by

† Email address for correspondence: A.J.Hogg@Bristol.ac.uk

Verhagen & van Wijngaarden (1965) and these bores may lead to high, but localized, impact pressures on the containing vessel.

Shallow fluid motion has often been modelled by the nonlinear shallow water equations [NSWE] (see, for example, Peregrine 1972). These are based upon the flow being predominantly parallel to the underlying boundary and thus fluid accelerations perpendicular to the boundary are negligible. This system of equations, which expresses mass and momentum conservation, has been applied widely to river and coastal flows (Peregrine 1972; Whitham 1974) as well as fluid sloshing problems (Armenio & Rocca 1996). Key features of the equations are that they model nonlinear wave motions, they may exhibit an unsteady interface between wetted and dry regions and, through discontinuous solutions (shocks), they capture the motion of the broken waves. There have been a number of algorithms proposed to compute the solutions numerically (see, for example, Leveque 2002), and the comparison of a range of solvers for one-dimensional unsteady flow presented by Zoppou & Roberts (2003). There are some tough challenges in computing these numerical solutions accurately and it is vital that results are validated by comparison with analytical solutions. The development of such a non-trivial test case is one of the outcomes of this study.

This work studies the impulsive motion of initially quiescent fluid over an inclined plane: we consider the flow of a shallow layer within a rigid rectangular cross-section flume that is tilted at some instant to generate an unsteady and spatially varying flow. This configuration provides insight to the early stages of a thin film of water sloshing within the tank and could be compared directly to laboratory observations. Analytical solutions of the nonlinear shallow water equations over an inclined boundary are relatively rare: Carrier & Greenspan (1958) found nonlinear, standing waves on a sloping beach, while Shen & Meyer (1963) developed a model of the run-up of a broken wave on a planar beach. More recently, Peregrine & Williams (2001) have generalized this analysis to calculate the overtopping that occurs if the flow is on a truncated beach and Pritchard, Guard & Baldock (2008) have calculated swash run-up and run-down on a planar beach. In this contribution, we demonstrate below that the presence of the endwalls of the flume adds significant complexity to the types of fluid motion that may be generated. In particular, we show that discontinuities develop at an interior location after a certain period following initiation, but that nevertheless we can calculate the position and magnitude of these shocks. Additionally we show that a moving interface forms between the wetted and dry regions in the flume.

The solutions we develop in this study are derived using analytical techniques that exploit the characteristic structure of the nonlinear shallow water equations. In certain regions where one of the characteristic variables is constant, we are able to track simply the evolution along characteristic curves. In regions where both characteristic variables vary we interchange the dependent and independent variables, a transformation that linearizes the governing equations. Thereafter we construct the solution using Riemann's method. This technique is described by Garabedian (1986) and has been recently used by Hogg (2006), Ancey *et al.* (2008) and Pritchard *et al.* (2008) to study frictionless inertial flows and by Kerswell (2005) to study Coulombic granular flows. As noted above, shallow flows up inclined boundaries have been modelled by Shen & Meyer (1963) and Peregrine & Williams (2001): both of these studies treated flows within unbounded domains, with idealized initial conditions, and developed solutions that did not form internal bores and featured a moving shoreline that progressed up the inclined plane before retreating offshore. In this study we show that the endwalls of the flume do influence the motion rather strongly and lead to

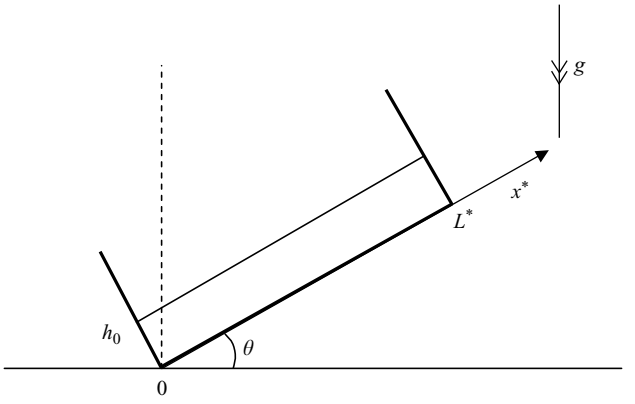

FIGURE 1. Initial configuration of the problem.

more complicated motions (including bores), for which the construct of the solutions require more sophisticated mathematical techniques.

The paper is structured as follows. We formulate the problem in § 2, identify the key dimensionless parameter, which is proportional to the length of the flume and present the governing equations in hodograph form. In § 3, we develop solutions for the motion at early times, identifying regions within which the characteristic variables are constant and varying, and we demonstrate how to construct the analytical solution using the method of characteristics and the Riemann representation of the flow. The latter is possible because under the hodograph transformation, the governing equations become linear. We also show when the techniques fail, potentially leading to multivalued regions, which are resolved by the introduction of discontinuous solutions. We show how to track the evolution of the discontinuous solutions in § 4 and we present some typical results. Finally, a summary and some conclusions are given in § 5.

2. Formulation of the problem

We consider a rectangular tank containing a shallow layer of water at rest, initially lying horizontally. The tank is suddenly tilted to generate a gravity-driven flow (see figure 1). Provided the layer is sufficiently shallow so that the ensuing motion is predominantly parallel with the underlying boundary and the pressure is hydrostatic, then the shallow water equations can be used to model the flow (Peregrine 1972). Aligning the x-axis with the direction along the tank, the following dimensional equations (starred variables) model the system (for further details, see Peregrine & Williams 2001):

$$\frac{\partial d^*}{\partial t^*} + \frac{\partial}{\partial x^*}(d^* u^*) = 0, \tag{2.1}$$

$$\frac{\partial u^*}{\partial t^*} + u^* \frac{\partial u^*}{\partial x^*} + g \cos\theta \frac{\partial d^*}{\partial x^*} = -g \sin\theta. \tag{2.2}$$

In these equations, d^* is the total water depth, u^* is the 'onshore' velocity, g is the gravitational acceleration and θ is the angle between the base of the tank and the horizontal direction. We choose a frame of reference in which the origin is at the left lower corner of the tank; the left wall of the tank is then located at $x = 0$, while the right one is at $x^* = L^*$. Finally, we assume that the tank is

instantaneously tilted at $t^* = 0$ and we consider the following initial configuration: $d^* = \text{constant} = h_0$ and $u^* \equiv 0$ (see figure 1). This initial condition, although in common with previous studies in this geometry, is idealized because we assume that there is no deformation of the free surface due to centrifugal accelerations, or other processes, during the tilting of the flume; essentially we require that there is no appreciable motion during the tilting, but that centrifugal accelerations also remain negligible. Denoting the time scale for tilting by T, there is no appreciable motion due to gravitational acceleration if $T \ll t_0 \equiv (h_0 \cos\theta/g)^{1/2}/\sin\theta$. Additionally we require that T is not so short that significant centrifugal accelerations develop: this requires that $T \gg t_r \equiv L^*\theta/(gh_0\cos\theta)^{1/2}$. Hence the regime within which the initial condition is accurate certainly demands that $t_r \ll t_0$ and hence when the inclination is small ($\theta \ll 1$), this leads to $\theta^2 \ll h_0/L^*$.

We can make system (2.1) dimensionless using the following scales:

$$x_0 = \frac{A}{\sin\theta}, \quad t_0 = \frac{1}{\sin\theta}\sqrt{\frac{A}{g}}, \quad u_0 = \sqrt{gA}, \quad d_0 = \frac{A}{\cos\theta}, \tag{2.3}$$

in which A is a proper vertical length. We choose $A = h_0\cos\theta$ so that we obtain $d_0 = h_0$. The dimensionless system is then given by

$$\frac{\partial d}{\partial t} + \frac{\partial}{\partial x}(d\,u) = 0, \tag{2.4}$$

$$\frac{\partial u}{\partial t} + u\frac{\partial u}{\partial x} + \frac{\partial d}{\partial x} = -1. \tag{2.5}$$

Using (2.3) we find the sole residual dimensionless parameter L that measures the length of the inclined tank relative to the initial fluid depth and the inclination of the flume, and is given by

$$L = \frac{L^*}{x_0} \equiv \tan\theta\frac{L^*}{h_0}. \tag{2.6}$$

It is noteworthy that under the scalings of (2.3), L emerges as the ratio of the flume inclination ($\tan\theta$) to the shallowness parameter (h_0/L^*). Alternatively it can be viewed as the ratio of the two vertical length scales, $L^*\sin\theta$ and $h_0\cos\theta$. We will show below that the magnitude of L determines the structure of the solutions and the locations at which discontinuous solutions first form. System (2.4) can be rewritten in characteristic form as follows:

$$\alpha \equiv u + t + 2c = \text{constant} \quad \text{along curves} \quad \frac{\mathrm{d}x}{\mathrm{d}t} = u + c, \tag{2.7a}$$

$$\beta \equiv u + t - 2c = \text{constant} \quad \text{along curves} \quad \frac{\mathrm{d}x}{\mathrm{d}t} = u - c, \tag{2.7b}$$

where $c = \sqrt{d}$ and α and β are the characteristic variables (Whitham 1974). It is straightforward to show that

$$u = \frac{\alpha + \beta}{2} - t \quad \text{and} \quad c = \frac{\alpha - \beta}{4}. \tag{2.8}$$

By adopting α and β as the independent variables instead of x and t (the hodograph transformation; Garabedian 1986), we find that (2.7*a*) and (2.7*b*) become

$$\frac{\partial x}{\partial \beta} = \left(\frac{3\alpha+\beta}{4} - t\right)\frac{\partial t}{\partial \beta} \quad \text{along curves such that} \quad \alpha = \text{constant}, \tag{2.9a}$$

$$\frac{\partial x}{\partial \alpha} = \left(\frac{\alpha+3\beta}{4} - t\right)\frac{\partial t}{\partial \alpha} \quad \text{along curves such that} \quad \beta = \text{constant}. \tag{2.9b}$$

This transformation is possible provided the Jacobian, $J = (\partial x/\partial\beta)(\partial t/\partial\alpha) - (\partial x/\partial\alpha)(\partial t/\partial\beta)$ is finite and non-zero. Combining together (2.9*a*) and (2.9*b*), we establish

$$\frac{\partial^2 t}{\partial\alpha\partial\beta} = \frac{3}{2(\alpha-\beta)}\left(\frac{\partial t}{\partial\alpha} - \frac{\partial t}{\partial\beta}\right). \tag{2.10}$$

We note that in terms of these hodograph variables, the nonlinear governing equations have become linear (Garabedian 1986; Hogg 2006) and that this will enable some of the analysis developed below.

3. The early stages solution

Before describing the method for integrating this problem, we first need to define the initial and boundary conditions for the configuration under examination (see figure 1) and introduce some notations. In terms of dimensionless variables, we have the initial condition $d = 1$ and $u = 0$ for $0 \leqslant x \leqslant L$ at $t = 0$, while the boundary conditions represent the impermeability of the endwalls of the tank and are given by $u = 0$ at $x = 0$ and $x = L$. Generally there could exist a specific instant $t_N^{(0)}$ when the water ceases to wet the right wall of the tank and a front curve $x_N = x_N(t)$ is generated. Then, we define the front curve x_N as the curve separating the wet part of the tank bottom from the dry part. At the front we have the kinematic conditions $\dot{x}_N = u$ and $c = 0$. Now, using the definition of x_N together with the definitions of α and β, we can rewrite the kinematic condition as $\dot{x}_N = \alpha - t$.

Given these conditions, we can solve the problem during the earliest time instants. We find the following regions in the (x, t)-plane: a constant state region U_1 within which α and β are constant, two simple wave regions S_1, S_2 within which one of α and β remains constant and two complex wave regions C_1 and C_2 within which α and β both vary (see figure 2). The boundaries between these region are demarked by the curves δ_1, γ_1 and γ_2, as explained below.

3.1. *Region* U_1

In this region the characteristic variables are given by $\alpha = 2$ and $\beta = -2$ and, therefore, $d = 1$, $u = -t$. The α- and β-characteristic curves (hereinafter denoted by the symbols γ and δ, respectively) are given by

$$\gamma : x(t) = x_0 + t - \frac{t^2}{2}, \quad \delta : x(t) = x_0 - t - \frac{t^2}{2}, \quad \text{with} \quad x_0 \in [0, L]. \tag{3.1}$$

Then region U_1 is bounded by the characteristic curves γ_1 and δ_1, emanating from $x = 0$ and $x = L$, respectively, and given by

$$\gamma_1 : x(t) = t - \frac{t^2}{2}, \quad \delta_1 : x(t) = L - t - \frac{t^2}{2}. \tag{3.2}$$

These curves intersect at $P_1 = (x_1, t_1) = (L/2(1 - L/4), L/2)$.

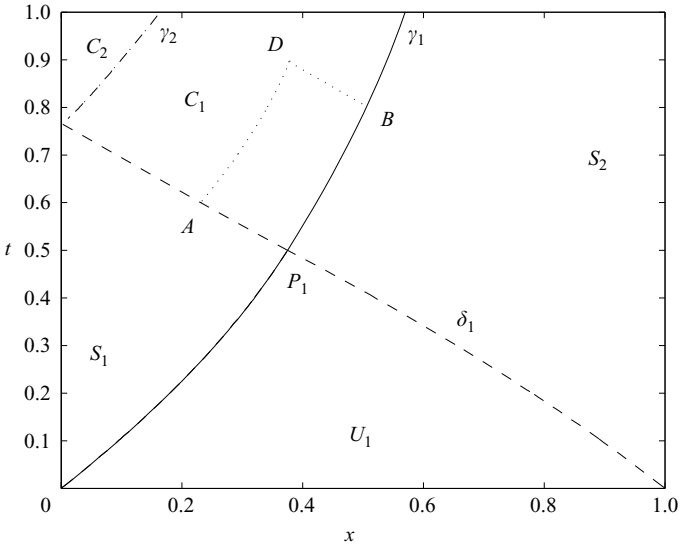

FIGURE 2. Sketch of regions U_1, S_1, S_2, C_1 and C_2 and the characteristic curves (γ_1, γ_2 and δ_1) that divide them for $L=1$. Also shown is the point $P_1=(x_1, t_1)$, where the characteristic curves γ_1 and δ_1 intersect and the points A, B and D that will be used to construct the solution within the region C_1.

3.2. *Region* S_1

Throughout this region $\beta=-2$, because all β-characteristics entering this region have originated in U_1. We start solving for the α-characteristics curves. From (2.7*a*), we find

$$\dot{x} = \frac{3\alpha}{4} - \frac{1}{2} - t, \tag{3.3}$$

and integrating we deduce that the α-characteristic curves are of the form

$$\gamma \,:\, x(t;\alpha) = x_0 + \left(\frac{3\alpha}{4} - \frac{1}{2}\right)(t-t_0) - \frac{t^2}{2} + \frac{t_0^2}{2}, \tag{3.4}$$

where t_0 and x_0 are constants. Since all γ-curves travel from the rigid wall into the region S_1, we demand that $x=0$ and $u=0$ at $t=t_0$. The former condition yields $x_0=0$, while from (2.8), the latter condition corresponds to $t_0=\alpha/2-1$ and thus (3.4) becomes

$$\gamma \,:\, x(t;\alpha) = \left(\frac{3\alpha}{4} - \frac{1}{2}\right)\left(t+1-\frac{\alpha}{2}\right) - \frac{t^2}{2} + \frac{(\alpha/2-1)^2}{2}. \tag{3.5}$$

Now we calculate $\alpha(x,t)$ by extracting α from (3.5) to find

$$\alpha(x,t) = 1 + \frac{3}{2}t \pm \frac{1}{2}\sqrt{(t+2)^2 - 16x}. \tag{3.6}$$

Since for $x=0$ we want α to satisfy $u=0$ (that is, $t=\alpha/2-1$), we have to choose the positive root. Substituting this expression in (2.7*b*), we obtain the following for the β-characteristic curves in the region S_1:

$$\delta \,:\, \dot{x} = -\frac{5}{8}(t+2) + \frac{1}{8}\sqrt{(t+2)^2 - 16x}. \tag{3.7}$$

This may be integrated to yield the following implicit solution (see appendix A for more details):

$$[\sqrt{(t+2)^2-16x}-2(t+2)]^2[\sqrt{(t+2)^2-16x}+3(t+2)]^3=2^9(5t_2+2)^2, \quad (3.8)$$

where the initial conditions are assigned along the curve γ_1, that is, $x=t_2-t_2^2/2$ for $0\leqslant t_2\leqslant t_1$. It is possible to expand (3.8) in the neighbourhood of the point $t=t_2$ to get an explicit solution. For $t_2<2/3$ we find (see appendix A)

$$x=\frac{(t+2)^2}{16}-\frac{1}{16}\left\{(2-3t_2)^2+2(9t_2+10)(t-t_2)+\left[\frac{(3t_2+14)(27t_2+14)}{(2-3t_2)^2}\right](t-t_2)^2\right\}+O\left(\left(t-\frac{2}{3}\right)^3\right),$$

while for $t_2=2/3$, we have

$$x=\frac{(t+2)^2}{16}-2\left(t-\frac{2}{3}\right)+\frac{\sqrt{2}}{3}\left(t-\frac{2}{3}\right)^{3/2}-\frac{5}{12}\left(t-\frac{2}{3}\right)^2+O((t-t_2)^3). \quad (3.9)$$

Thus it has become apparent that the value $t_2=2/3$ seems to represent a special case for solution (3.8). The reason may be revealed as follows: for the α-characteristics given by (3.5), we have $t_0=\alpha/2-1$ and we can rewrite (3.5) using the parameter t_0 instead of α to get

$$\gamma: x(t;t_0)=\left(\frac{3}{2}t_0+1\right)(t-t_0)-\frac{t^2}{2}+\frac{t_0^2}{2}. \quad (3.10)$$

All these curves start travelling inside S_1 from the rigid wall at $t=t_0$. Note that their 'steepness' $(3/2\,t_0+1)$ grows as t_0 becomes larger and so there could be particular values of t_0 such that different γ-curves meet together. In this case the solution becomes multivalued and this may be interpreted as breaking and subsequent shock formation (see, for example, Whitham 1974). The condition for the coalescence of the two γ-curves is that $\partial x/\partial t_0=0$. Thus we find that this occurs at

$$t=\frac{2}{3}(1+2t_0). \quad (3.11)$$

The expression in (3.11) gives the time $t\equiv t(t_0)$ at which an *envelope* of γ-curves occurs. Inverting (3.11), we obtain $t_0=t_0(t)$; then, substituting such expression in (3.10), we get the explicit expression of the envelope

$$x=\frac{(t+2)^2}{16}. \quad (3.12)$$

In figure 3 we show the envelope path together with the full path of γ_1. Such curves delimit a multivalued region M between S_1 and U_1. In this figure we have assumed $L\geqslant 4/3$ so that the curve δ_1 does not intersect γ_1 before the multivalued solutions first arise. We are interested in the first instant, t_s at which breaking occurs. Using (3.11), we establish

$$t_s=\min_{t_0\in[0,+\infty)}\left[\frac{2}{3}(1+2t_0)\right]=\frac{2}{3}. \quad (3.13)$$

This result explains why $t_2=2/3$ is a special value for solution (3.8), because it marks the start of the multivalued region M. Finally, substituting t_s in (3.12), we obtain the

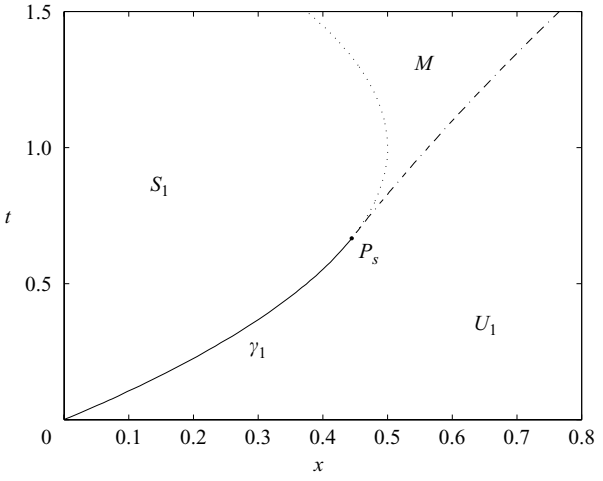

FIGURE 3. Regions of the (x, t)-plane when $L \geqslant 4/3$. U_1, S_1 and M denote the uniform region ($\alpha = 2, \beta = -2$), the simple wave region ($\beta = -2$) and the region within which multivalued solutions occur, respectively. The characteristic curve, γ_1 is plotted upto P_s with a solid line and is continued with a dotted line. The envelope of multivalued solutions is plotted with a dot-dash line.

point P_s where breaking first occurs

$$P_s = (x_s, t_s) = \left(\frac{4}{9}, \frac{2}{3}\right). \tag{3.14}$$

Note that P_s lies on the curve γ_1. The occurrence of multivaluedness occurs within S_1 if $t_s < t_1$ and this implies that $L > 4/3$. However if $L < 4/3$ then $t_s > t_1$ and multiplicity occurs within the region C_1.

Before proceeding to the analysis of regions S_2 and C_1, it is useful to find the solution for t as function of the characteristic variable invariants α and β. Since in S_1, $\beta = -2$, the solution may be denoted by $t = t(\alpha, -2)$. The first step is to compute the α-derivative of (3.5)

$$\frac{\mathrm{d}x}{\mathrm{d}\alpha} = \left(\frac{3\alpha}{4} - \frac{1}{2} - t\right)\frac{\mathrm{d}t}{\mathrm{d}\alpha} + \frac{3}{4}t - \frac{\alpha}{2} + \frac{1}{2}. \tag{3.15}$$

Then, using (2.9*b*), we find

$$\left(\frac{\alpha}{2} + 1\right)\frac{\mathrm{d}t}{\mathrm{d}\alpha} = -\frac{(3t + 2 - 2\alpha)}{4}, \tag{3.16}$$

which gives the following solution:

$$t(\alpha, -2) = \frac{2\alpha - 6}{5} + \frac{c_0}{(\alpha + 2)^{3/2}}, \tag{3.17}$$

where c_0 is a constant of integration. Note that we are integrating along the δ-curves on which $\beta = -2$. Such curves start travelling inside S_1 from the boundary curve γ_1 where $\alpha = 2$. Then, the initial condition is $t(2, -2) = t_2$ and we immediately obtain

$$t(\alpha, -2) = \frac{2\alpha - 6}{5} + 8\left(t_2 + \frac{2}{5}\right)(\alpha + 2)^{-3/2}. \tag{3.18}$$

Finally, we can evaluate $x(\alpha, -2)$ using (2.9*b*) and the condition $x(2, -2) = t_2 - t_2^2/2$

$$x(\alpha, -2) = -\frac{3}{100}(\alpha+2)^2 - \frac{32}{25}\frac{(5t_2+2)^2}{(\alpha+2)^3} + \frac{14}{25}\frac{(5t_2+2)}{(\alpha+2)^{1/2}}. \tag{3.19}$$

These expressions will be used below in the evaluation of the solution within C_1: in particular we will employ the values of $t(\alpha, -2)$ emanating from $t_2 = t_1 = L/2$. It is noteworthy that the multiplicity described above can be observed in these expressions: both $\partial t/\partial\alpha$ and $\partial x/\partial\alpha$ vanish when $\alpha = 2$ and $t_2 = 2/3$.

3.3. *Region* S_2

Throughout this region $\alpha = 2$, because all of the α-characteristics entering this domain have originated in U_1 (see figure 2). Similarly to the analysis of the previous section, we first find the paths of the β-characteristics. From (2.7*b*), we establish

$$\dot{x} = \frac{1}{2} + \frac{3\beta}{4} - t, \tag{3.20}$$

which may be integrated to obtain

$$\delta : x(t;\beta) = x_3 + \left(\frac{1}{2} + \frac{3\beta}{4}\right)(t - t_3) - \frac{t^2}{2} + \frac{t_3^2}{2}. \tag{3.21}$$

Since all β-characteristics travel from the rigid wall at the right-hand end of the tank, into the region S_2, we have $x = L$ and $u = 0$ at $t = t_3$. Thus we deduce $x_3 = L$ and from (2.8), the latter condition corresponds to $t_3 = 1 + \beta/2$. Thus (3.21) becomes

$$\delta : x(t;\beta) = L + \left(\frac{1}{2} + \frac{3\beta}{4}\right)\left(t - 1 - \frac{\beta}{2}\right) - \frac{t^2}{2} + \frac{(1+\beta/2)^2}{2}. \tag{3.22}$$

Now we can find $\beta(x, t)$ by extracting β from (3.22). We find

$$\beta(x, t) = -1 + \frac{3}{2}t - \frac{1}{2}\sqrt{(2-t)^2 - 16(x-L)}. \tag{3.23}$$

Substituting such expression in (2.7*a*), we obtain

$$\gamma : \dot{x} = \frac{5}{4} - \frac{5}{8}t - \frac{1}{8}\sqrt{(2-t)^2 - 16(x-L)}. \tag{3.24}$$

This may be integrated to give the α-characteristic path in region S_2. Following a procedure similar to that applied in appendix A, we find an implicit solution for (3.24). However, in this case it will be more useful to construct the solutions $t(2, \beta)$ and $x(2, \beta)$. Similarly to the analysis used for region S_1, we find that

$$t(2, \beta) = \frac{6 + 2\beta}{5} + 8\left(t_4 - \frac{2}{5}\right)(2-\beta)^{-3/2}, \tag{3.25}$$

and

$$x(2, \beta) = L - \frac{3}{100}(2-\beta)^2 - \frac{32}{25}\frac{(5t_4-2)^2}{(2-\beta)^3} - \frac{14}{25}\frac{(5t_4-2)}{(2-\beta)^{1/2}}, \tag{3.26}$$

where t_4 parameterizes the starting point of these α-characteristics on the curve δ_1, such that $0 \leqslant t_4 \leqslant t_1$. The region S_2 is bounded to the left in the (x, t)-plane by the continuation of the curve γ_1, which is the α-characteristic emanating from the origin. This curve is given in parametric form by substituting $t_4 = t_1 = L/2$ into (3.25) and

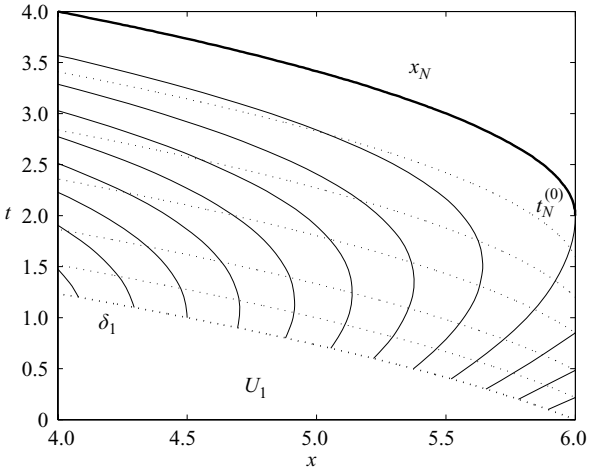

FIGURE 4. The front curve x_N (thick solid line), the α-characteristic curves (thin solid lines) and the β-characteristic curves (dotted lines) as functions of time inside the simple wave region S_2 for $L = 6$.

(3.26). Thus we find that γ reaches the rigid wall at the far right of the tank ($x = L$) at $\beta = 2 - (32 - 80t_1)^{2/5}$, which corresponds to times t_w given by

$$t_w = 2 - 2^{3/5}(2 - 5t_1)^{2/5}. \tag{3.27}$$

Note that if $t_1 > 2/5$ and thus $L > 4/5$ then γ_1 does not reach this endwall. Conversely if $L < 4/5$, then after γ_1 reaches the endwall, there is a complicated pattern of simple and complex wave regions in the (x, t)-plane arising from the reflection of this characteristic.

Finally we examine whether these solutions lead to a multivalued region. We rewrite (3.22) as function of t_3 only

$$\delta : x(t;\beta) = L + \left(\frac{3t_3}{2} - 1\right)(t - t_3) - \frac{t^2}{2} + \frac{t_3^2}{2}. \tag{3.28}$$

As in region S_1, the 'steepness' $(3/2\,t_3 - 1)$ increases as t_3 increases and following the standard procedure of determining when $\partial x/\partial t_3 = 0$, we find that the envelope of the δ-curves is given by

$$x(t) = L + \frac{1}{16}(t - 2)^2. \tag{3.29}$$

This envelope lies outside of the tank and thus there is no multivalued region; rather inside S_2 there is a fan of β-characteristic curves.

We also note that inside S_2, the flow depth is $d = (\alpha - \beta)^2/16 = (2 - \beta)^2/16$ and, thus, when $\beta = 2$, the depth vanishes and a front between the wet and dry regions, x_N, is generated. The instant $t_N^{(0)}$ at which the front starts to move is obtained using the impermeability condition at the right rigid wall; we immediately find $t_N^{(0)} = 1 + \beta/2 = 2$. Thereafter the motion of x_N is readily calculated since $\alpha = \beta = 2$ and thus we obtain

$$\dot{x}_N = \alpha - t = 2 - t, \quad \Rightarrow \quad x_N = L - 2 + 2t - \frac{t^2}{2} \quad \text{for } t > 2. \tag{3.30}$$

Figure 4 shows the front curve x_N and the α- and β-characteristic curves for $L = 6$, noting that the plotted behaviour is typical for all tanks of sufficient length so that

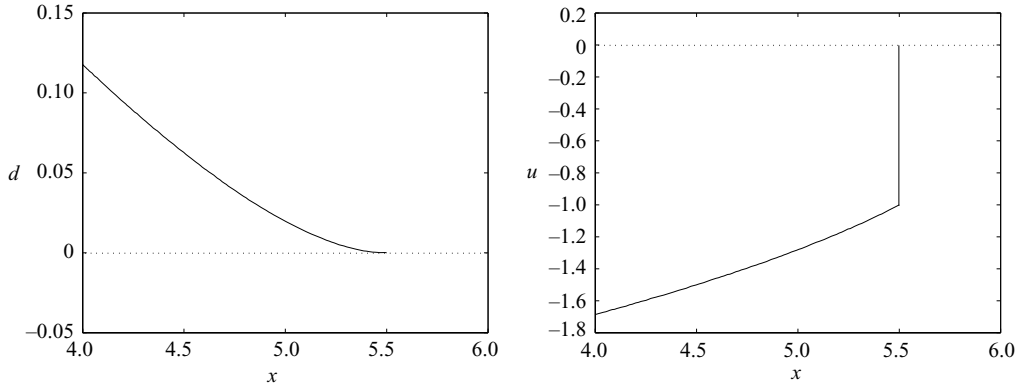

FIGURE 5. The height $d(x,t)$ and velocity $u(x,t)$, as functions of x, near the front of the motion at $t=3$ for $L=6$.

the regions S_2 and C_1 remain distinct at $t=2$ (i.e. $L>4/5$). Profiles of the depth and velocity fields close to the interface between the wetted and dry regions are plotted in figure 5. Note that for this case $L=6$ and at $t=3$, the interface between the wet and dry regions of the flume lies at $x_N(3)=11/2$.

3.4. *Region C_1*

In this region it is no longer possible to solve the problem by simply integrating along the characteristic curves, because both characteristic variables are changing. Thus a more sophisticated method is required. We interchange dependent and independent variables and thus seek solutions of the form $t(\alpha,\beta)$ and $x(\alpha,\beta)$. Furthermore we introduce the Riemann function, $B=B(a,b;\alpha,\beta)$, which satisfies the partial differential equation adjoint to (2.10) and given by

$$\frac{\partial^2 B}{\partial a\,\partial b}+\frac{3}{2\,(a-b)}\left(\frac{\partial B}{\partial a}-\frac{\partial B}{\partial b}\right)-\frac{3\,B}{(a-b)^2}=0, \tag{3.31}$$

subject to the boundary conditions

$$\frac{\partial B}{\partial b}=\frac{-3\,B}{2\,(a-b)}\ \text{along}\ a=\alpha,\quad \frac{\partial B}{\partial a}=\frac{3\,B}{2\,(a-b)}\ \text{along}\ b=\beta,\quad B(\alpha,\beta;\alpha,\beta)=1. \tag{3.32}$$

For this partial differential equation, the Riemann function is given by Garabedian (1986)

$$B(a,b;\alpha,\beta)=\frac{(a-b)^3}{(a-\beta)^{3/2}\,(\alpha-b)^{3/2}}\,F\left[\frac{3}{2},\frac{3}{2};1;\frac{(a-\alpha)(\beta-b)}{(a-\beta)(\alpha-b)}\right], \tag{3.33}$$

where F is the hypergeometric function. Then the Riemann construction applies to regular domains, $\mathscr{D}$ with boundaries $\partial\mathscr{D}$ in the (α,β)-hodograph plane (see Garabedian 1986; Hogg 2006). Explicitly we require that

$$\int_{\partial D}\omega=0, \tag{3.34}$$

where $\omega = -V\,\mathrm{d}a + U\,\mathrm{d}b$, and

$$V = \frac{3\,t\,B}{2\,(a-b)} + \frac{B}{2}\,\frac{\partial t}{\partial a} - \frac{t}{2}\,\frac{\partial B}{\partial a}, \tag{3.35a}$$

$$U = -\frac{3\,t\,B}{2\,(a-b)} + \frac{B}{2}\,\frac{\partial t}{\partial b} - \frac{t}{2}\,\frac{\partial B}{\partial b}. \tag{3.35b}$$

We are now in the position to solve the problem in region C_1. We consider the Riemann's function $B = B(a, b; \alpha, \beta)$ and the square P_1ADB in the hodograph plane made up by segments of the characteristic curves and depicted in figure 2. The coordinates of the points in the (α, β)-plane are

$$A = (\alpha, -2), \quad B = (2, \beta), \quad D = (\alpha, \beta) \quad \text{and} \quad P_1 = (2, -2). \tag{3.36}$$

The functions $t(2, \beta)$ and $t(\alpha, -2)$ along the characteristics γ_1 and δ_1 are known through (3.18) and (3.25), respectively, and therefore the only unknown variable is $t(\alpha, \beta)$ at D. Applying Riemann's method to the characteristic square and integrating by parts, we get

$$\int_{P_1B} \omega = \int_{-2}^{\beta} U|_{a=2}\,\mathrm{d}b = \frac{1}{2}\left[B(2, \beta; \alpha, \beta)\,t(2, \beta) - B(2, -2; \alpha, \beta)\,t(2, -2)\right] - \int_{-2}^{\beta} t(2, b)\left[\frac{3\,B}{2(a-b)} + \frac{\partial B}{\partial b}\right]\Bigg|_{a=2} \mathrm{d}b, \tag{3.37a}$$

$$\int_{AP_1} \omega = \int_{2}^{\alpha} V|_{b=-2}\,\mathrm{d}a = \frac{1}{2}\left[B(\alpha, -2; \alpha, \beta)\,t(\alpha, -2) - B(2, -2; \alpha, \beta)\,t(2, -2)\right] + \int_{2}^{\alpha} t(a, -2)\left[\frac{3\,B}{2(a-b)} - \frac{\partial B}{\partial a}\right]\Bigg|_{b=-2} \mathrm{d}a, \tag{3.37b}$$

which are known functions since $t(2, \beta)$ and $t(\alpha, -2)$ along AP_1 and P_1B, respectively, are known. Integrating by parts and using the boundary condition in (3.32), we also have

$$\int_{BD} \omega = -\int_{2}^{\alpha} V|_{b=\beta}\,\mathrm{d}a = -\frac{1}{2}\left[t(\alpha, \beta) - B(2, \beta; \alpha, \beta)\,t(2, \beta)\right], \tag{3.38a}$$

$$\int_{DA} \omega = , \int_{\beta}^{-2} U|_{a=\alpha}\,\mathrm{d}b = \frac{1}{2}\left[B(\alpha, -2; \alpha, \beta)\,t(\alpha, -2) - t(\alpha, \beta)\right]. \tag{3.38b}$$

Combining together the previous results, we obtain

$$t(\alpha, \beta) = B(2, \beta; \alpha, \beta)\,t(2, \beta) + B(\alpha, -2; \alpha, \beta)\,t(\alpha, -2) - B(2, -2; \alpha, \beta)\,t(2, -2) + \int_{2}^{\alpha} t(a, -2)\left[\frac{3\,B}{2(a-b)} - \frac{\partial B}{\partial a}\right]\Bigg|_{b=-2} \mathrm{d}a - \int_{-2}^{\beta} t(2, b)\left[\frac{3\,B}{2(a-b)} + \frac{\partial B}{\partial b}\right]\Bigg|_{a=2} \mathrm{d}b. \tag{3.39}$$

Once $t(\alpha, \beta)$ is known, we can obtain $x(\alpha, \beta)$ from the relations in (2.9a, b). Here, we give the solution for $x(\alpha, \beta)$ in the general case. We integrate (2.9a) between β_0 and β and (2.9b) between α_0 and α (α_0 and β_0 are arbitrary starting points) and combine

these results to obtain

$$x(\alpha,\beta) = x(\alpha_0,\beta_0) + \frac{3\beta+\alpha}{4}\,t(\alpha,\beta) - \frac{3\alpha_0+\beta_0}{4}\,t(\alpha_0,\beta_0) + \frac{\alpha_0-\beta}{2}\,t(\alpha_0,\beta) - \frac{1}{4}\left[\int_{\alpha_0}^{\alpha} t(a,\beta)\,\mathrm{d}a + \int_{\beta_0}^{\beta} t(\alpha_0,b)\,\mathrm{d}b\right] - \frac{t^2(\alpha,\beta)}{2} + \frac{t^2(\alpha_0,\beta_0)}{2}, \tag{3.40}$$

where $t(\alpha,\beta)$, $t(\alpha_0,\beta)$, $t(\alpha_0,\beta_0)$ and $x(\alpha_0,\beta_0)$ are known.

The region C_1 is bounded to the left in the (x,t)-plane by the α-characteristic γ_2 emanating from the t-axis from the point at which the curve δ_1 reaches $x=0$ (see figure 2). This reflection changes the nature of the solution, because while within C_2 both α and β continue to vary, this region is bounded to the left by $x=0$ at which the rigid wall conditions demand that $u=0$ and $t=\alpha+\beta$. In principle the solution may be constructed using Riemann's method, but this will not be pursued in this paper, for which the focus is the initial evolution of the flow.

In figure 6 we show the analytical solutions for d and u at various fixed times and $L=1$, noting that the characteristic curve δ_1 reaches $x=0$ at $t=0.766$. In figures 6(a) and 6(b) $t=1/4$ and the solutions spread over the regions S_1, U_1 and S_2. In figures 6(c) and 6(d) we choose the special case $t=1/2$ when the region U_1 disappears and the regions S_1 and S_2 touch each other at the point P_1. Finally, in figures 6(e) and 6(f) $t=2/3$ and the solutions spread over the regions S_1, C_1 and S_2. Note that, even if d and u are always continuous, there is a jump in their derivatives while crossing different regions.

The steepening of the profiles in figures 6(e) and 6(f) suggests that the solution is tending towards a state in which it has become multivalued and thereafter forms a shock wave. In figure 6 $L<4/3$ and so as discussed above, we anticipate that this shock wave occurs within the region C_1. Moreover, breaking occurs along the curve γ_1 (by which we mean approaching the curve γ_1 from the region C_1) where both the x- and t-derivatives of u and d are discontinuous. Far from this being a special case, similar behaviour was observed by Greenspan (1958) for waves propagating shoreward on a plane frictionless beach. To find where the shock first occurs, we study the coordinates transformation from the (α,β)-plane to the (x,t)-plane in a generic complex region. We have

$$\begin{cases} \dfrac{\partial}{\partial\alpha} = \dfrac{\partial x}{\partial\alpha}\dfrac{\partial}{\partial x} + \dfrac{\partial t}{\partial\alpha}\dfrac{\partial}{\partial t}, \\ \dfrac{\partial}{\partial\beta} = \dfrac{\partial x}{\partial\beta}\dfrac{\partial}{\partial x} + \dfrac{\partial t}{\partial\beta}\dfrac{\partial}{\partial t}, \end{cases} \quad\Longrightarrow\quad \begin{cases} \dfrac{\partial}{\partial t} = \dfrac{1}{J}\dfrac{\partial x}{\partial\beta}\dfrac{\partial}{\partial\alpha} - \dfrac{1}{J}\dfrac{\partial x}{\partial\alpha}\dfrac{\partial}{\partial\beta}, \\ \dfrac{\partial}{\partial x} = -\dfrac{1}{J}\dfrac{\partial t}{\partial\beta}\dfrac{\partial}{\partial\alpha} + \dfrac{1}{J}\dfrac{\partial t}{\partial\alpha}\dfrac{\partial}{\partial\beta}, \end{cases} \tag{3.41}$$

where $J=(\partial x/\partial\beta)(\partial t/\partial\alpha)-(\partial x/\partial\alpha)(\partial t/\partial\beta)$ is the Jacobian of the transformation. Such a transformation does not apply in simple wave regions since one of the state variables (α or β) is identically constant. A continuous wave arising in a hyperbolic quasi-linear system of equations (such as the NWSE) loses its continuity and becomes a shock wave when its derivatives becomes unbounded. From (3.41), we observe that this happens at the first time instant at which $J=0$. After such an instant we can no longer apply the coordinate transformation in (3.41) since the one-to-one correspondence between the (α,β)-plane and the (x,t)-plane is lost. Using (2.9a,b), we obtain $J=2c\,(\partial t/\partial\alpha)(\partial t/\partial\beta)$ and, therefore, $J=0$ if and only if $c=0$, $\partial t/\partial\alpha=0$ and/or $\partial t/\partial\beta=0$. The first condition confirms the shoreline to be a singular curve for the NSWE while the other conditions give the breaking conditions in the complex region.

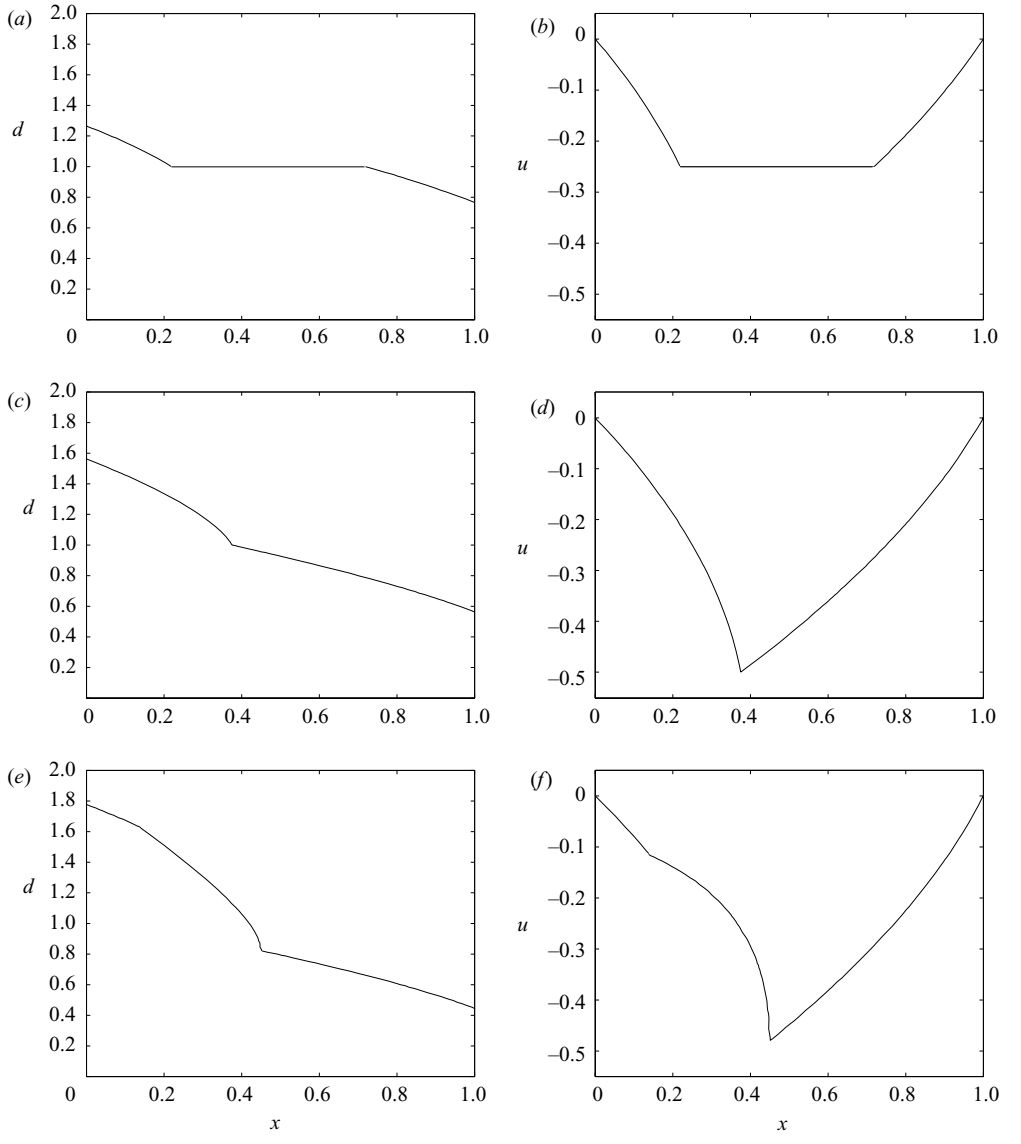

FIGURE 6. The depth d and velocity u as functions of x at different times for $L=1$: (a) and (b) represent d and u at $t=1/4$; (c) and (d) represent d and u at $t=1/2$; (e) and (f) represent d and u at $t=2/3$.

From (3.39) we evaluate

$$\left.\frac{\partial t}{\partial \alpha}\right|_{\alpha=2} = \frac{-3}{2(2-\beta)} t(2,\beta) + \frac{2}{(2-\beta)^{3/2}} - \frac{3}{4(2-\beta)^{3/2}} \int_{-2}^{\beta} \frac{t(2,b)}{(2-b)^{1/2}}\, \mathrm{d}b. \tag{3.42}$$

This may be further simplified by substituting $t(2,\beta)$ from (3.25) to obtain

$$\left.\frac{\partial t}{\partial \alpha}\right|_{\alpha=2} = \frac{1}{10(2-\beta)^{5/2}} \left[6(2+5\beta) - 15(10+\beta)t_1\right] + \frac{2}{5}. \tag{3.43}$$

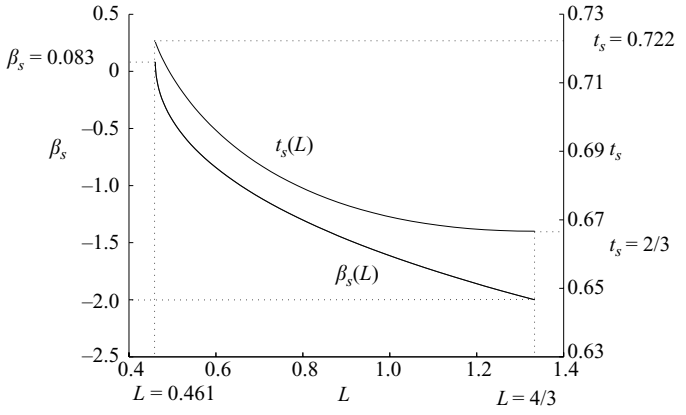

FIGURE 7. The value of the characteristic variable β_s and the time t_s at which the multivalued region starts within C_1 as a function of the dimensionless length of the flume, L. Note that the multivalued region only starts within C_1 when $0.461 < L < 4/3$.

Thus we may determine when $\partial t/\partial\alpha(2, \beta)$ first vanishes, marking the start of the multivalued region. We plot the variation of this value of $\beta \equiv \beta_s$ and the corresponding time of the shock formation $t_s = t(2, \beta_s)$ as functions of the dimensionless length of the tank, L (figure 7). We note that when $L = 4/3$ the derivative $\partial t/\partial\alpha$ first vanishes at $\beta_s = -2$ ($t_s = t_1 = 2/3$), which is in agreement with the above analysis. Smaller values of L lead to the multivalued region starting in C_1: when $L = 1$, $\partial t/\partial\alpha$ vanishes at $\beta_s = -1.614$, which corresponds to $t_s = 0.671$. Thus the profiles plotted in figure 6 at $t = 2/3$ are close to the first time at which this method of solution breaks down and discontinuous solutions form.

We also note that when $L < 0.4607$ there is no value of β_s for which $\partial t/\partial\alpha$ vanishes on the characteristic $\alpha = 2$. This indicates that there is no shock formed within the region C_1. However, there is a stronger constraint on the formation of a multivalued region in C_1: we require the multivalued region to form before the curve γ_1 reaches the endwall ($x = L$) (i.e. $t_s \leqslant t_w$). We calculate that the limiting case of $t_s = t_w$ occurs when $\beta = -0.5879$, $t_1 = 0.2653$ and $t_s = t_w = 0.7060$. Thus for $L < 0.5306$, we determine that no shock forms within C_1 before the region interacts with the endwall and forms more complicated pattern of simple and complex wave regions which is beyond the scope of this paper.

4. A shock solution

In this section, we introduce and illustrate an analytical expression for the shock motion when $L > 4/3$. In this situation, the shock is generated by the coalesence α-characteristic curves while the β-characteristics jump across the discontinuity. This implies that behind the shock we can no longer assume $\beta = -2$ and we have to assume the existence of a complex wave region C_s. As will be demonstrated in § 4.1, such a region is bounded by the shock itself and by the β-characteristic crossing the starting breaking point P_s (hereinafter denoted by δ_s). A simple sketch of C_s is drawn in figure 8. In front of the shock is the region U_1 where $\alpha = 2$ and $\beta = -2$. The following relations are used to define the jump of the physical quantities, expressing

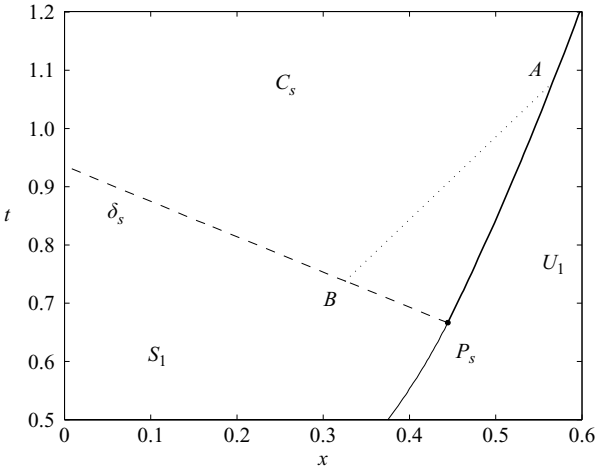

FIGURE 8. Sketch of the shock wave (thick solid line) in the (x, t)-plane, the β-characteristic through $P_s \equiv (4/9, 2/3)$ (dashed line) and the regions U_1, S_1 and C_s. The dotted line denotes the α-characteristic curve used in the construction of the solution using Riemann's method. In this plot $L = 3.5$.

conservation of mass and momentum across the shock:

$$s\,[d] \;=\; [Q], \tag{4.1a}$$

$$s\,[Q] \;=\; \left[\frac{d^2}{2} + \frac{Q^2}{d}\right], \tag{4.1b}$$

where $s = \mathrm{d}x_s/\mathrm{d}t$ is the shock velocity, $Q = ud$ and the bracket symbol $[f] = f_2 - f_1$ represents the jump across the shock (subindices 1 and 2 indicating the quantity in front and behind the shock, respectively). Then, since Q_1 and d_1 are in U_1, we also have $Q_1 = -t$ and $d_1 = 1$.

4.1. *Preliminary results*

It is very simple to show that the shock wave has zero strength at P_s, that is, all the quantities are continuous at P_s. First of all, we note that the shock wave has to develop inside the multivalued region, that is, between the α-characteristic γ_1 and the envelope in (3.12). At P_s these curves both give $\dot{x} = 1/3$ and then $s = 1/3$. We substitute $[Q]$ from (4.1a) into (4.1b) and solve for d_2: the only positive solution is $d_2 = 1 = d_1$. So we have $[d] = [Q] = 0$. These results have very important consequences. First of all no β-rarefaction fan starts from P_s since $[\beta] = [u] - 2[c] = 0$ and, then, the slope of the β-characteristic changes continuously behind the shock. This also implies that the β-characteristic crossing P_s (hereinafter denoted by δ_s) is known and is given by (3.7) along with the initial condition $x = 4/9$ at $t = 2/3$. The absence of rarefaction waves confirms our initial assumptions on the boundary of the region C_s.

4.2. *A hodographic approach*

We assume the quantities just behind the shock to be continuous and employ the hodograph variables introduced by Carrier & Greenspan (1958) to represent them in the phase space. We define $d = \sigma^2/16$ and $u = \lambda/2 - t$. (Note that the quantities in front of the shock originate from the uniform wave region U_1 given by the point $(\sigma, \lambda) = (4, 0)$.) This new set of variables offer advantages in simplifying the analysis that follows; in particular we find that the trajectory of the shock wave

is parameterized by sole variable σ. The new variables are related to the original characteristic quantities by

$$\alpha = \frac{\lambda + \sigma}{2}, \quad \beta = \frac{\lambda - \sigma}{2}. \tag{4.2}$$

Using the variables σ and λ, the starting set of equations (2.4) becomes

$$\begin{cases} \dfrac{\partial x}{\partial \sigma} - u\dfrac{\partial t}{\partial \sigma} + c\dfrac{\partial t}{\partial \lambda} = 0 \\ \dfrac{\partial x}{\partial \lambda} - u\dfrac{\partial t}{\partial \lambda} + c\dfrac{\partial t}{\partial \sigma} = 0, \end{cases} \Rightarrow \begin{cases} \dfrac{\partial \xi}{\partial \sigma} = \dfrac{\lambda}{2}\dfrac{\partial t}{\partial \sigma} - \dfrac{\sigma}{4}\dfrac{\partial t}{\partial \lambda} \\ \dfrac{\partial \xi}{\partial \lambda} = \dfrac{\lambda}{2}\dfrac{\partial t}{\partial \lambda} - \dfrac{\sigma}{4}\dfrac{\partial t}{\partial \sigma}, \end{cases} \tag{4.3}$$

where $\xi = x + t^2/2$. Extracting s from (4.1*a*) and substituting in (4.1*b*), we obtain

$$[Q]^2 = [d]\left[\frac{d^2}{2} + \frac{Q^2}{d}\right]. \tag{4.4}$$

Since we have

$$d_1 = 1, \quad u_1 = -t, \quad d_2 = \frac{\sigma^2}{16}, \quad u_2 = \frac{\lambda}{2} - t, \tag{4.5}$$

substituting such expressions in (4.4) leads to the following curve in the (σ, λ)-space:

$$\lambda(\sigma) = \pm\frac{\sqrt{2\sigma^2 + 32}\,(\sigma^2 - 16)}{16\sigma}. \tag{4.6}$$

Substituting back into (4.1*a*), we obtain

$$s = \pm\frac{\sigma\sqrt{2\sigma^2 + 32}}{32} - t. \tag{4.7}$$

Since P_s corresponds to $(\sigma, \lambda) = (4, 0)$ and, at this point, $t = 2/3$ and $s = 1/3$, we deduce that the positive root is the right choice. Finally, we can write (4.7) as follows:

$$\frac{\mathrm{d}x_s}{\mathrm{d}t} = \frac{\sigma\sqrt{2\sigma^2 + 32}}{32} - t. \tag{4.8}$$

Since all the quantities are defined along the curve in (4.6), we can consider σ as an independent variable and this yields

$$\frac{\mathrm{d}x_s}{\mathrm{d}\sigma} = \left[\frac{\sigma\sqrt{2\sigma^2 + 32}}{32} - t_s\right]\frac{\mathrm{d}t_s}{\mathrm{d}\sigma}, \tag{4.9}$$

or, in a more compact form

$$\frac{\mathrm{d}\xi_s}{\mathrm{d}\sigma} = \left[\frac{\sigma\sqrt{2\sigma^2 + 32}}{32}\right]\frac{\mathrm{d}t_s}{\mathrm{d}\sigma}. \tag{4.10}$$

Since $\mathrm{d}\xi/\mathrm{d}\sigma = \partial\xi/\partial\sigma + \dot{\lambda}\,\partial\xi/\partial\lambda$, where $\dot{\lambda} = \mathrm{d}\lambda/\mathrm{d}\sigma$, then combining (4.3) with (4.10), we obtain

$$\frac{\mathrm{d}t_s}{\mathrm{d}\sigma} = -\frac{\sigma^2}{2\sqrt{2\sigma^2 + 32}}\left(\frac{\partial t}{\partial \lambda} + \dot{\lambda}\frac{\partial t}{\partial \sigma}\right). \tag{4.11}$$

To solve the problem, we need to know $\partial t/\partial\sigma$ and $\partial t/\partial\lambda$ evaluated along $\lambda(\sigma)$. For this purpose, we use the Riemann's method described in Hogg (2006).

4.3. *Solution*

We consider the triangle ABP_s shown in figure 8. The curve AB is an α-characteristic curve (the specific value of α is used as a parameter, as explained below), while the curve BP_s is the β-characteristic passing through P_s (along it $\beta = -2$ and α is assumed to be known as well). Finally, the curve P_sA represents the shock curve, which forms the right-hand boundary to the complex region C_s (i.e. along the curve $\lambda(\sigma)$ in (4.6)).

However, to use the Riemann's method, we have to express the curve $\lambda(\sigma)$ (given in (4.6) as function of σ only) as function of either α or β. Using (4.2) and (4.6), it is easy to show that $\mathrm{d}\alpha/\mathrm{d}\sigma > 0$. Then we choose α as the independent variable assuming the curve $\lambda(\sigma)$ to be expressed through a curve $\beta(\alpha)$ in the (α, β)-plane. Finally, using (3.34), we get

$$\int_{ABP_s} \omega = \int_{AB} \omega + \int_{BP_s} \omega + \int_{P_sA} \omega = 0. \tag{4.12}$$

The coordinates of points A, B and P_s in the hodograph plane are

$$A = (\alpha, \beta(\alpha)), \qquad B = (\alpha, -2), \qquad P_s = (2, -2). \tag{4.13}$$

Using the boundary condition in (3.32), the first integral gives

$$\int_{AB} \omega = \int_{\beta(\alpha)}^{-2} U|_{a=\alpha}\, \mathrm{d}b = \frac{t(\alpha, -2) - B(\alpha, \beta(\alpha); \alpha, -2)\, t(\alpha, \beta(\alpha))}{2}, \tag{4.14}$$

while the second one is

$$\int_{BP_s} \omega = -\int_{\alpha}^{2} V|_{b=-2}\, \mathrm{d}a = \frac{t(\alpha, -2) - B(2, -2; \alpha, -2)\, t(2, -2)}{2}. \tag{4.15}$$

The last integral is evaluated along the curve $\beta = \beta(\alpha)$ and, therefore, it is given by

$$\int_{P_sA} \omega = \int_{2}^{\alpha} [U\,\dot{b} - V]|_{b=b(a)}\, \mathrm{d}a, \tag{4.16}$$

where $\dot{b} = \mathrm{d}b/\mathrm{d}a$. The global result is

$$t(\alpha, -2) - \frac{1}{2}\,[B(2, -2; \alpha, -2)\, t(2, -2) + B(\alpha, \beta(\alpha); \alpha, -2)\, t(\alpha, \beta(\alpha))] + \int_{2}^{\alpha} [U\,\dot{b} - V]\Big|_{b=b(a)}\, \mathrm{d}a = 0. \tag{4.17}$$

First we note that $t(\alpha, -2)$ and $B(2, -2; \alpha, -2)$ are taken along the characteristic curve δ_s and, hence, they are known. We denote them with $f_1(\alpha)$ and $f_2(\alpha)$, respectively. Moreover we also know that $t(2, -2) = 2/3$. Then (4.17) becomes

$$f_1(\alpha) - \frac{f_2(\alpha)}{3} - \frac{B\big(\alpha, \beta(\alpha); \alpha, -2\big)\, t\big(\alpha, \beta(\alpha)\big)}{2} + \int_{2}^{\alpha} \big[\, U\,\dot{b} - V\,\big]\,\Big|_{b=b(a)}\, \mathrm{d}a = 0. \tag{4.18}$$

Now we need to express such equation as a function of σ. The functions $f_1(\alpha)$ and $f_2(\alpha)$ may be written as $\hat{f}_1(\sigma) = f_1(\alpha(\sigma))$ and $\hat{f}_2(\sigma) = f_2(\alpha(\sigma))$ since $\alpha(\sigma)$ is known along the shock curve. All the other quantities are directly defined along the shock curve and, therefore, they can be written as functions of σ using (4.2) together with (4.6). In particular we have $t(\alpha, \beta(\alpha)) \equiv t_s(\sigma)$. In order to parameterize the integration along the shock inside the integral (4.16), we introduce the variables ρ and τ such

that, according to (4.2), we have

$$B(a,b;\alpha,-2)\Big|_{b=b(a)} = B\left(\frac{\tau(\rho)+\rho}{2},\frac{\tau(\rho)-\rho}{2};\frac{\lambda(\sigma)+\sigma}{2},-2\right). \tag{4.19}$$

It follows immediately that

$$B\big(\alpha,\beta(\alpha);\alpha,-2\big) = B\left(\frac{\lambda(\sigma)+\sigma}{2},\frac{\lambda(\sigma)-\sigma}{2};\frac{\lambda(\sigma)+\sigma}{2},-2\right) \equiv B(\sigma), \tag{4.20}$$

and thus we may write

$$\int_2^\alpha [U\dot{b}-V]|_{b=b(a)}\mathrm{d}a = \int_4^\sigma \left[U\frac{\mathrm{d}b}{\mathrm{d}\rho}-V\frac{\mathrm{d}a}{\mathrm{d}\rho}\right]\mathrm{d}\rho$$
$$= \int_4^\sigma \left\{\frac{t_s}{2}\left[\frac{\partial B}{\partial\tau}+\dot{\tau}\frac{\partial B}{\partial\rho}-\dot{\tau}\frac{3B}{\rho}\right]-\frac{B}{2}\left[\frac{\partial t}{\partial\tau}+\dot{\tau}\frac{\partial t}{\partial\rho}\right]\right\}\mathrm{d}\rho. \tag{4.21}$$

Further, denoting

$$F(\sigma) = \hat{f}_1(\sigma)-\frac{2}{3}\hat{f}_2(\sigma), \qquad D(\sigma) = B(\sigma)\left[\frac{1}{2}-\frac{\sqrt{2\sigma^2+32}}{\sigma^2}\right], \tag{4.22}$$

using (4.11) and integrating by parts, we can rewrite (4.18) in the following way:

$$t_s(\sigma) = \frac{F(\sigma)}{D(\sigma)}+\frac{1}{D(\sigma)}\int_4^\sigma t_s\left\{\frac{1}{2}\left[\frac{\partial B}{\partial\tau}+\dot{\tau}\frac{\partial B}{\partial\rho}-\dot{\tau}\frac{3B}{\rho}\right]-\frac{\mathrm{d}}{\mathrm{d}\rho}\left[B\frac{\sqrt{2\rho^2+32}}{\rho^2}\right]\right\}\mathrm{d}\rho.$$

Now simplifying the argument of the integral, we can write

$$t_s(\sigma) = \frac{F(\sigma)}{D(\sigma)}+\frac{1}{D(\sigma)}\int_4^\sigma t_s\left\{c_1(\rho)\frac{\partial B}{\partial\tau}+c_2(\rho)\frac{\partial B}{\partial\rho}+c_3(\rho)B\right\}\mathrm{d}\rho. \tag{4.23}$$

where

$$c_1(\rho) = \frac{\rho^4-8\rho^2-128}{4\rho^4}, \quad c_2(\rho) = \frac{\rho^4-8\rho^2-128}{8\rho^2\sqrt{2\rho^2+32}}, \quad c_3(\rho) = -\frac{3\rho^4+8\rho^2-128}{8\rho^3\sqrt{2\rho^2+32}}.$$

Equation (4.23) is a Volterra equation of the second kind and it can be solved by successive iterations. We note that some care is required in its numerical solution because $F, D \to 0$ as $\sigma \to 4$ and for consistency we require that $t_s = 2/3$ at $\sigma = 4$. We demonstrate in appendix B that there are no singularities in the integral equation and that its formulation is consistent with the initial condition.

All the results presented up to here, are valid as long as the shock motion depends only on regions S_1 and U_1. This occurs during the first stages of evolution but after a sufficiently long time, the shock is also influenced by other regions and thereafter solution (4.23) is no longer valid. The construction can fail in the following two ways.

First, the complex wave region, C_1 is bounded by the curve δ_s and when this β-characteristic reaches $x = 0$, it is reflected as a forward-propagating α-characteristic, which eventually reaches the shock wave at the point P_3. Thereafter the shock starts to self-interact since it meets the β-characteristics reflected at the t-axis that have previously crossed the shock. As a consequence (4.23) holds up to P_3 while a more complicated expression is needed for the further shock evolution. We may determine the point P_3 in the (σ,λ)-plane by first finding when the characteristic, δ_s first reaches $x = 0$. From the results of appendix A, this may be calculated as $t = t_2 = 0.9608$. In

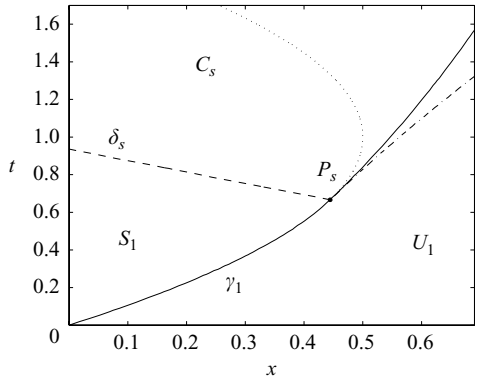

FIGURE 9. The trajectory of the shock curve in the (x, t)-plane (thick solid line), together with the β-characteristic passing, δ_1), (dashed line), the α-characteristic, γ_1 before P_s (thin solid line) and after P_s (dotted line) and the envelope of multiple curve (dashed-dotted line). In these plots, $L = 3.5$.

terms of the characteristic variables, $\beta = -2$, while $\alpha \equiv \alpha_2 = 2(t_2 + 1) = 3.9216$. Thus in the (σ, λ)-plane

$$P_2 = (\sigma_2, \lambda_2) = (5.9216, 1.9216)\,. \tag{4.24}$$

Thereafter we integrate along the α-characteristic to find where it intersects the shock. This occurs at point P_3, which is given by

$$P_3 = (\sigma_3, \lambda_3) = (5.8681, 1.9719), \quad \Leftrightarrow \quad P_3 = (\alpha_3, \beta_3) = (\alpha_2, -1.9481). \tag{4.25}$$

The second way in which the constructed solution (4.23) may fail is if the shock wave crosses the curve δ_1 before reaching the point P_3. After that, the front of the shock wave is influenced by region S_2. The point P_3 is given by (0.7016, 1.6207) in the (x, t)-plane. Since the curve δ_1 passes through this point when $L = 3.6356$, we deduce that the construction fails by the shock waves reaching the simple wave region S_2 if $4/3 < L < 3.6356$, whereas for $L \geqslant 3.6356$ the shock wave begins to self-interact.

In all figures that follow, we calculate the solutions when $L = 3.5$ so that eventually this construction fails via the first of the possibilities described above. In figure 9 we show the shock curve as obtained by the numerical solution of (4.23). The computed solution is very accurate since it satisfies the shock relations with a maximum error of about 3×10^{-5}. In figure 9 we also show the shock path together with the envelope given in (3.12) and the continuation of γ_1. It is evident that the shock 'cuts' the multivalued region M in two parts: the part in front of the shock is included in U_1, the part behind is included in C_s.

Figures 10 (a) and 10(b) show the solution $t_s(\sigma)$ of (4.23) and the associated solution $x_s(\sigma)$ obtained through (4.9). Moreover, figures 10 (c), 10(d) and 10(e) show respectively the jump of the quantities d, u and Q along the shock wave while in figure 10(f) the shock velocity s is plotted. It is evident that the shock is growing in magnitude as it develops and that its forward motion is progressively slowing. Finally, to illustrate clearly the shock evolution, in figure 11 the discontinuous solutions of d and u are plotted at fixed times. At $t = 2/3$ the shock wave is just generated while at $t = 0.9608$ the discontinuity is completely evident inside the domain. We chose $t = 0.9608$ since for $t > 0.9608$ the region C_2 starts to develop near the left rigid wall.

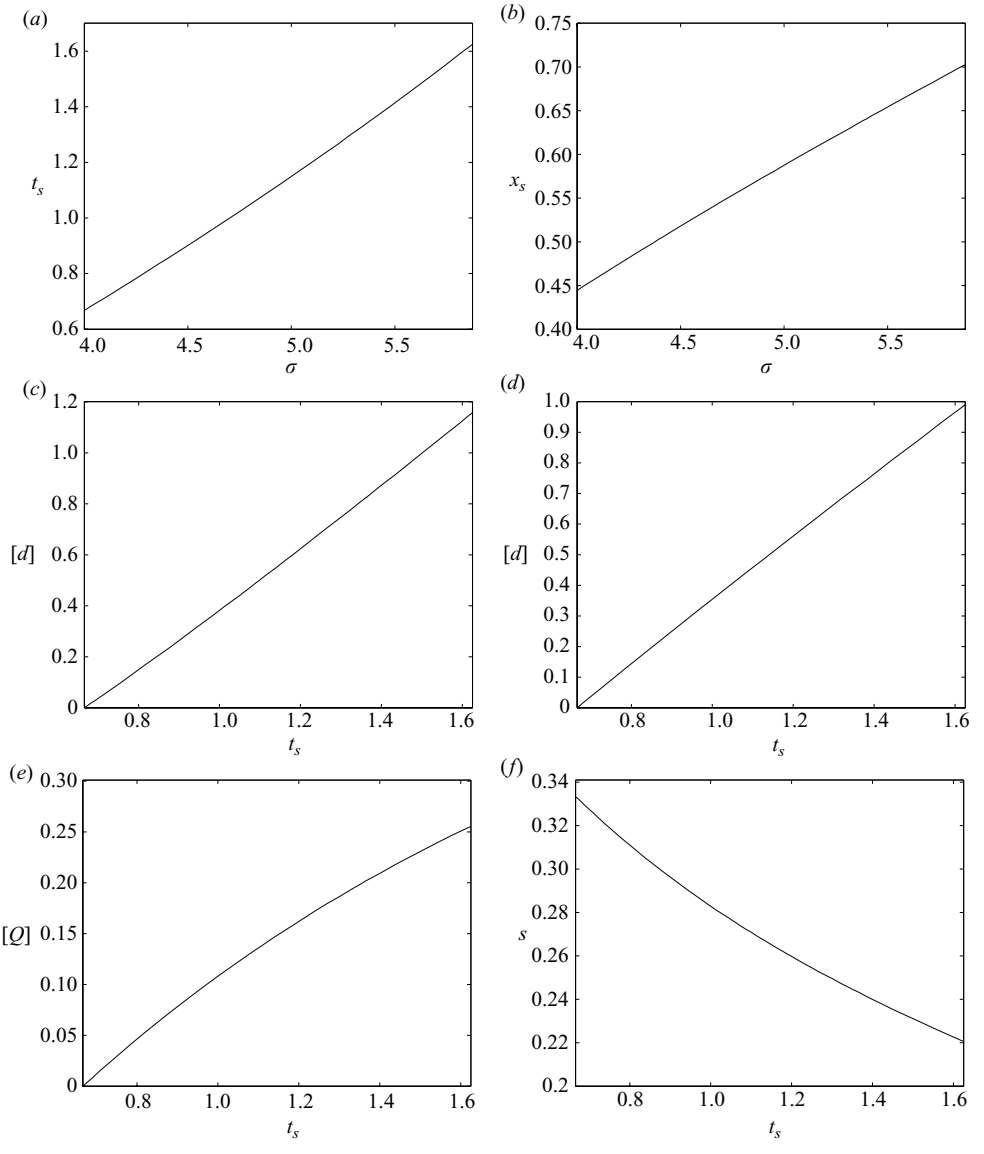

FIGURE 10. (a, b) The trajectory of the shock as functions of σ; (c, d, e) the jumps of d, u and Q across the shock wave and (f) the shock velocity s as a function of time. In these plots, $L = 3.5$.

5. Summary and conclusions

In this paper we have constructed analytical solutions for the two-dimensional motion of an initially static shallow layer of fluid within an inclined tank. In this description of the motion, there is a single dimensionless parameter L which measures the length of the tank relative to the initial depth of fluid and the inclination of the tank (see (2.6)). The magnitude of this parameter determines the character of the fluid motions that occur en route to attaining the final static state when the free surface has become horizontal.

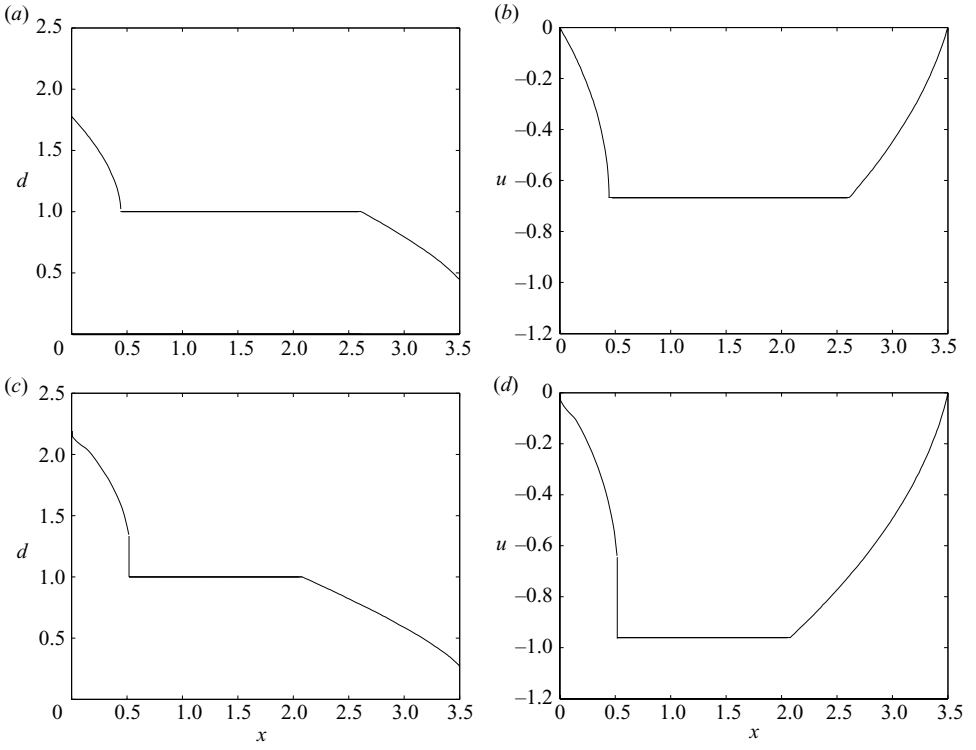

FIGURE 11. The depth $d(x,t)$ and velocity $u(x,t)$ of the shallow layer as function of distance along the flume x, at times (a,b) $t=2/3$ and (c,d) $t=0.9608$ for $L=3.5$

In these calculations we have shown how the initial stages of the motion feature uniform and simple waves regions within which one, or both of the characteristic variables are constant. Here, the velocity and height fields are evaluated relatively straightforwardly using the method of characteristics. However the presence of the endwalls of the flume introduce further complexities into the motion and thus the flow features regions within which both characteristic variables vary. Nevertheless we may still calculate the depth and velocity by adopting hodograph variables and implementing the Riemann construction for the solution to the governing equations. This follows the approach of Hogg (2006) for dam-break flows over horizontal surfaces in which the presence of an impermeable back wall also strongly modified the flow.

We find that the solution develops discontinuities (bores) at relatively early times. This emerges from the coalescence of different forward-propagating characteristics and its precise location of initial formation depends upon L. Tracking the evolution and motion of the discontinuity requires special treatment; in this contribution we have demonstrated how to construct the solution either side of the moving discontinuity and how to link them by applying jump conditions to determine the evolution of its location and magnitude. Additionally we have shown that the flow develops a moving interface between the wet and dry regions at the end of the flume and we have calculated when this forms and how the motion subsequently progresses. Our description is limited to relatively early dimensionless times. Subsequent motion could be modelled using this construction, but careful account would need to be

made of the boundaries between the regions and the reflections that occur when characteristics reach the boundaries.

Shallow water equations have been widely used in near-shore hydrodynamics and for modelling the nonlinear sloshing of containers partially filled with liquid. The numerical integration of the equations can be a significant challenge since the solutions may feature discontinuities and moving contact points between wet and dry regions. It is therefore vital to have analytical solutions, against which the numerical solutions can be validated. As well as providing insight into nonlinear wave motion, this study adds significantly to the available test cases, because it provides analytical solutions to an experimentally realizable configuration, which is spatially and temporally varying and which generates bores after some initial development.

Appendix A. Characteristic curves within region S_1

We integrate (3.7) by first defining a new variable $q \equiv q(t)$ such that

$$x = \frac{(t+2)^2}{16}(1-q^2). \tag{A 1}$$

Thus differential equation (3.7) becomes

$$\frac{q}{q^2+q-6}\frac{\mathrm{d}q}{\mathrm{d}t} = -\frac{1}{(t+2)}, \tag{A 2}$$

which, once integrated, gives the following implicit solution:

$$\left(\frac{q-2}{q_2-2}\right)^{2/5}\left(\frac{q+3}{q_2+3}\right)^{3/5} = \frac{(t_2+2)}{(t+2)}, \tag{A 3}$$

where t_2 and q_2 are the initial conditions. Since all the δ-curves start from inside S_1 on the curve γ_1, the initial values x_2 and t_2 are linked by the relationship, $x_2 = t_2 - t_2^2/2$. Then, we obtain

$$q_2 = \frac{1}{(t_2+2)}\sqrt{(t_2+2)^2 - 16\,x_2} = \frac{|3\,t_2-2|}{t_2+2}. \tag{A 4}$$

Finally, because $3t_0 - 2 \leqslant 0$, we find

$$[\sqrt{(t+2)^2-16x} - 2(t+2)]^2\,[\sqrt{(t+2)^2-16x} + 3(t+2)]^3 = 2^9\,(5t_2+2)^2. \tag{A 5}$$

Since it is not possible to get an exact explicit analytical solution of (3.7), we try to obtain an approximate solution by expanding (A 5) in a neighbourhood of $t = t_2$. This will be useful for the numerical solutions obtained in this paper. First, defining the new variables $y = y(t)$ and $z = z(t)$ such that:

$$y = \sqrt{(t+2)^2-16x}, \qquad z = t - t_2, \tag{A 6}$$

we rewrite (A 5) as follows:

$$[y - 2z - 2(t_2+2)]^2\,[y + 3z + 3(t_2+2)]^3 = 2^9\,(5t_2+2)^2. \tag{A 7}$$

Then, we assume the following expansion for y:

$$y = a_0 + a_1\sqrt{z} + a_2 z + a_3 z^{3/2} + a_4 z^2 + O(z^{5/2}), \tag{A 8}$$

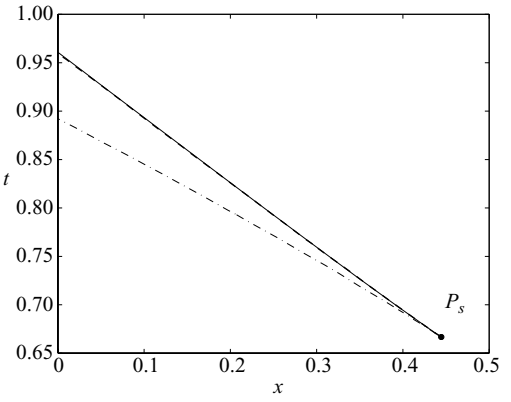

FIGURE 12. Solutions of (3.7): numerical solution (solid line) and the approximate solutions $x^{(-)}$ (dotted-dashed line) and $x^{(+)}$ (dashed thick line).

where $a_0 = 2 - 3t_2$ in virtue of the chosen initial condition. Substituting (A 8) into (A 7) and collecting together the same orders of magnitude of $\sqrt{z}$, we get

$$a_1 = a_3 = a_5 = 0, \quad a_2 = \frac{9t_2 + 10}{2 - 3t_2}, \quad a_4 = -24\,\frac{5t_2 + 2}{(2 - 3t_2)^3}, \tag{A 9}$$

for $t_0 < 2/3$ and

$$a_0 = 0, \quad a_1 = \pm 4\sqrt{2}, \quad a_2 = -\frac{2}{3}, \quad a_3 = \pm\frac{7}{18}\sqrt{2}, \quad a_4 = \frac{7}{270}, \tag{A 10}$$

for $t_0 = 2/3$. Note that in the latter case we find two distinct solutions. This is consequence of the generation of the shock wave at $t = 2/3$. Substituting (A 9) into (A 8), we find approximate solution (3.8). However, substituting (A 10) into (A 8), we find two solutions

$$x^{(\pm)}(t) = \frac{(t+2)^2}{16} - 2\left(t - \frac{2}{3}\right) \pm \frac{\sqrt{2}}{3}\left(t - \frac{2}{3}\right)^{3/2} - \frac{5}{12}\left(t - \frac{2}{3}\right)^2 + O\left(\left(t - \frac{2}{3}\right)^3\right). \tag{A 11}$$

One of these solutions is spurious, arising as a consequence of the shock wave singularity. A simple way to determine which of the solutions is to be retained is to compare $x^{(+)}$ and $x^{(-)}$ with the numerically evaluated implicit solution (A 5) (figure 12). Here we see that $x^{(+)}$ is the relevant solution as it is almost indistinguishable from the exact numerical solution.

Appendix B. Regularity of Volterra equation (4.23)

To verify that (4.23) has no singularities, we need to study its behaviour when the shock just starts, that is, for $t \to 2/3$. Indeed, such a limit is not trivial since $t \to 2/3$ corresponds to $\sigma \to 4$ and in this case we have both $D(\sigma) \to 0$ and $F(\sigma) \to 0$. Keeping in mind that $B(\sigma) \to 1$ as $\sigma \to 4$ and using a Taylor expansion, it is easy to show that

$$D(\sigma) = \frac{3}{16}(\sigma - 4) + O((\sigma - 4)^2). \tag{B 1}$$

Now denoting $I(\rho;\sigma) = \{c_1(\rho)\, B_\tau + c_2(\rho)\, B_\rho + c_3(\rho)\, B\}$, we also obtain

$$\int_4^\sigma t_s(\rho)\, I(\rho;\sigma)\mathrm{d}\rho = -\frac{1}{8}(\sigma-4) + O\big((\sigma-4)^2\big). \tag{B 2}$$

Finally we need to evaluate $F(\sigma)$ in the regime $|\sigma-4| \ll 1$. Using (3.33) and (4.2), we establish that $\alpha = 2 + (\sigma-4) + \cdots$ and thus

$$\hat{f}_1(\sigma) = \frac{2}{3} + O((\sigma-4)^2), \qquad \hat{f}_2(\sigma) = 1 - \frac{3}{8}(\sigma-4) + O((\sigma-4)^2). \tag{B 3}$$

Hence $F(\sigma) = (\sigma-4)/4 + \cdots$ and then

$$t_s = \frac{F}{D} - \frac{1}{D}\int_4^\sigma t_s I(\rho;\sigma)\, \mathrm{d}\rho = \frac{2}{3} + O\left((\sigma-4)\right), \tag{B 4}$$

and this is consistent with the initial time $t_s = 2/3$ at $\sigma = 4$.

REFERENCES

Ancey, C., Iverson, R. M., Rentschler, M. & Denlinger, R. P. 2008 An exact solution for ideal dam-break floods on steep slopes. *Water Resour. Res.* **44**, W01430. doi:10.1029/2007WR006353.

Armenio, V. & Rocca, M. L. 1996 On the analysis of sloshing of water in rectangular containers: numerical study and experimental validation. *Ocean Engng* **8**, 705–739.

Carrier, G. F. & Greenspan, H. P. 1958 Water waves of finite amplitude on a sloping beach. *J. Fluid Mech.* **4**, 97–109.

Faltinsen, O. M., Landrini, M. & Greco, M. 2004 Slamming in marine applications. *J. Engng Math* **48**, 187–217.

Garabedian, P. R. 1986 *Partial Differential Equations.* Chelsea Publishing.

Greenspan, H. P. 1958 On the breaking of water waves of finite amplitude on a sloping beach. *J. Fluid Mech.* **4**, 330–334.

Hogg, A. J. 2006 Lock-release gravity currents and dam-break flows. *J. Fluid Mech.* **569**, 61–87.

Huang, Z. & Hsiung, C. 1996 Nonlinear shallow-water flow on deck. *J. Ship Res.* **40**, 303–315.

Kerswell, R. R. 2005 Dam break with Coulomb friction: a model for granular slumping? *Phys. Fluids* **17**, 057101(1–16).

Lee, T., Zhou, Z. & Cao, Y. 2002 Numerical simulations of hydraulic jumps in water sloshing and water impacting. *J. Fluids Engng* **124**, 215–226.

Leveque, R. J. 2002 *Finite Volume Methods for Hyperbolic Problems*, 558 pp. Cambridge.

Peregrine, D. H. 1972 Equations for water waves and the approximations behind them. In *Waves on Beaches and Resulting Sediment Transport* (ed. R. Meyer), chapter 3, pp. 95–121. Academic Press.

Peregrine, D. H. & Williams, S. M. 2001 Swash overtopping a truncated plane beach. *J. Fluid Mech.* **440**, 391–399.

Pritchard, D., Guard, P. A. & Baldock, T. E. 2008 An analytical model for bore-driven run-up. *J. Fluid Mech.* **610**, 183–193.

Shen, M. C. & Meyer, R. E. 1963 Climb of a bore on a beach. Part 3. Run-up. *J. Fluid Mech.* **16**, 113–125.

Verhagen, J. H. G. & van Wijngaarden, L. 1965 nonlinear oscillations of fluid in a container. *J. Fluid Mech.* **22**, 737–751.

Whitham, G. B. 1974 *Linear and Nonlinear Waves*, 636 pp. Wiley.

Zoppou, C. & Roberts, S. 2003 Explicit schemes for dam-break simulations. *J. Hydr. Engng* **129**, 11–34.